

## *Supplementary Information*

# **Directed Evolution of Excited State Lifetime and Brightness in FusionRed using a Microfluidic Sorter**

*Premashis Manna<sup>1</sup>, Sheng-Ting Hung<sup>1</sup>, Srijit Mukherjee<sup>1,2</sup>, Pia Friis<sup>1</sup>, David M. Simpson<sup>3</sup>, Maria Lo<sup>3</sup>, Amy E. Palmer<sup>2,3</sup>, Ralph Jimenez<sup>1,2</sup>*

<sup>1</sup>JILA, NIST, and University of Colorado, Boulder, Colorado 80309, United States

<sup>2</sup>Department of Chemistry and Biochemistry, University of Colorado, Boulder, Colorado 80309, United States

<sup>3</sup>BioFrontiers Institute, University of Colorado, Boulder, Colorado 80309, United States

**Table of contents:**

<b>Section</b>	<b>Title</b>
Sec. 1	Excited state Lifetime and Fluorescence Quantum Yield of Fluorescent Proteins
Sec. 2	Microfluidic Design and Manifold Assembly
Sec. 3	Schematic of the Optical Set-up
Sec. 4	Schematic of the Electronics and Signal Processing
Sec. 5	Comparative Screening Results Using Linear and Logarithmic Amplifier for Signal Amplification
Sec. 6	Theory of Frequency-Domain Lifetime Measurements in Flow Cytometry
Sec. 7	Protocol for Random and Site-directed Mutagenesis
Sec. 8	Characterization of the Single Mutants of FR-13
Sec. 9	Evolution of FR-13 Mutant
Sec. 10	Sequence Alignment of the FusionRed Mutants
Sec. 11	Photo-physics of the FusionRed Mutants
Sec. 12	FACS Screening of Cells Expressing FusionRed Mutants
Sec. 13	Maturation Kinetics and Expression level of RFPs
Sec. 14	OSER Assay
Sec. 15	Program for Analyzing OSER Structures

## Sec. 1. Excited state Lifetime and Fluorescence Quantum Yield of Fluorescent Proteins

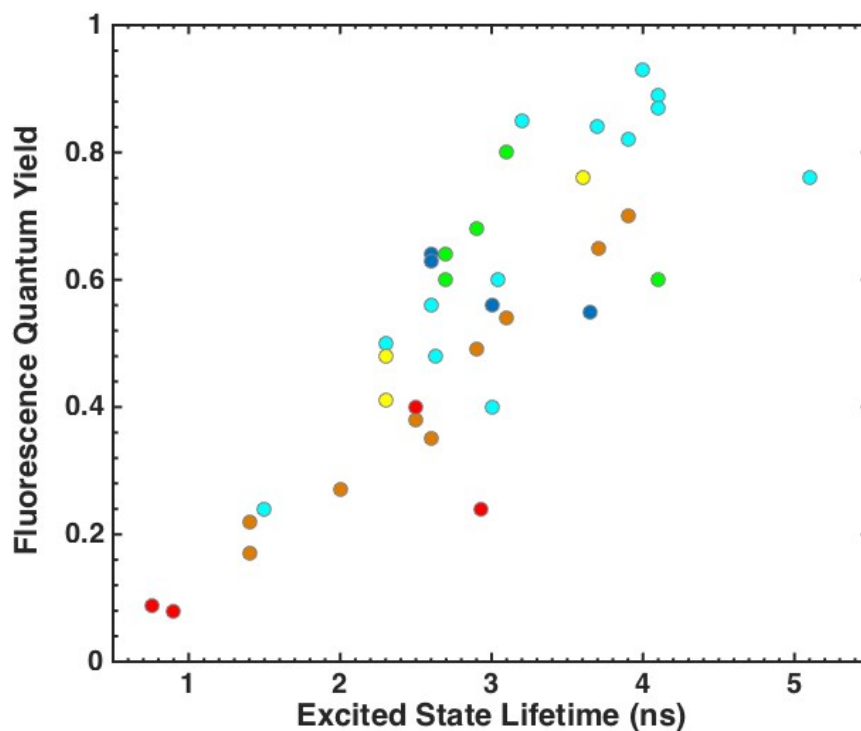


Figure S1: The plot of fluorescence quantum yield vs. excited state lifetime of fluorescent proteins (FPs) reveals a positive correlation between these two photo-physical parameters. Values of lifetime and quantum yield of FPs were obtained from [www.fpbases.org](http://www.fpbases.org). Blue, cyan, yellow, orange and red dots represent the corresponding emission properties of the FPs.

The correlation between fluorescence quantum yield ( $\phi$ ) and excited state lifetime ( $\tau$ ) forms the basis of our microfluidic selection of FP mutants ( $\phi = k_r \cdot \tau$ , where  $k_r$  is radiative rate constant)<sup>1</sup>. Selection of mutants with longer excited state lifetime would ensure higher fluorescence quantum yield which in turn would enhance the molecular brightness of the FPs.

## Sec. 2. Microfluidic Design and Manifold Assembly

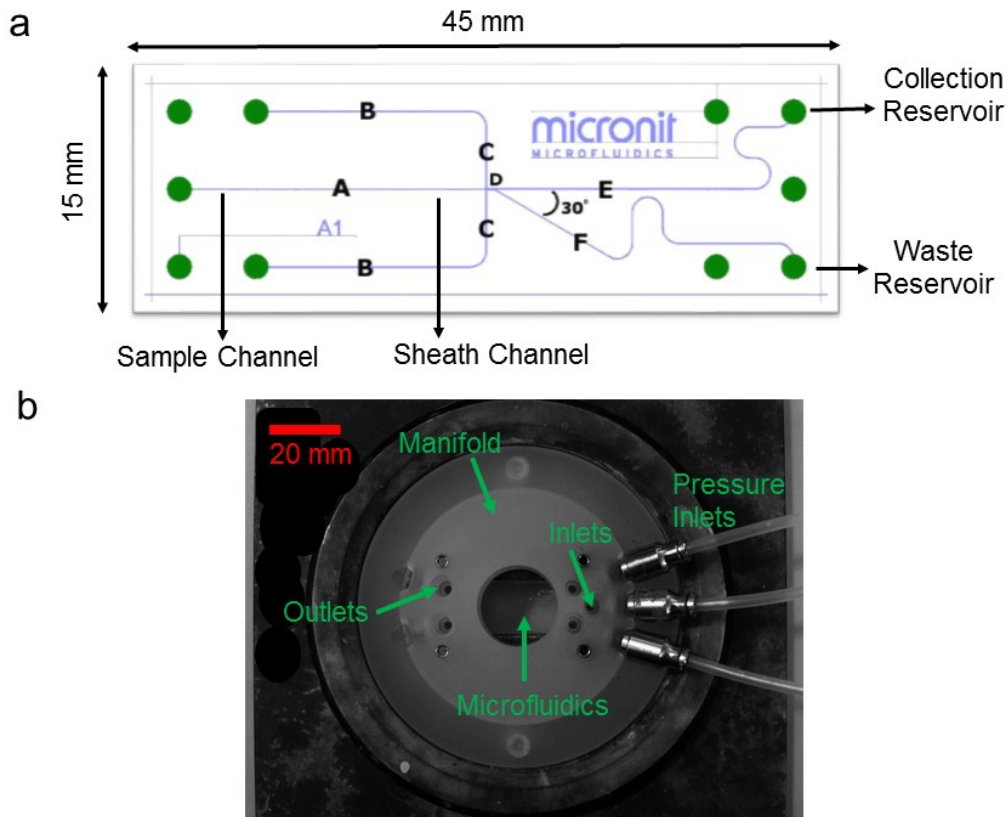


Figure S2: **(a)** Design of the microfluidic chip. The chip is custom fabricated by Micronit Microtechnologies B.V., The Netherlands. The lengths and widths of different portions of the channels are: A [20 mm, 100 μm], B [15 mm, 130 μm], C [5 mm, 130 μm], D [0.5 mm, 150 μm], E [27 mm, 125 μm], F [27 mm, 125 μm]. The height of all channels is wet-etched to 25 μm. Solutions with cells are flowed in the middle channel (A). Sheath channels (B) hydrodynamically focus the sample channel to produce a narrow stream that improves the coefficient of variation (CV) of the measurements. (D) is the interrogation region where multiple laser beams are focused. (E) and (F) are collection and waste channels respectively. **(b)** Microfluidic and manifold (made of polytetrafluoroethylene, PTFE) assembly consisting of three inlets (sheath, sample, sheath) and two outlets (waste and collection). The pressure of each channel is independently controlled by pressure controllers (Pneutronics, OEM, EPS10-5-0-2) within 0-2 psi range. The microfluidic chip is entirely made of borosilicate glass and fits in the middle of the manifold allowing delivery of light for epi- and trans-illuminations<sup>2,3</sup>.

### Sec. 3. Schematic of the Optical Set-up

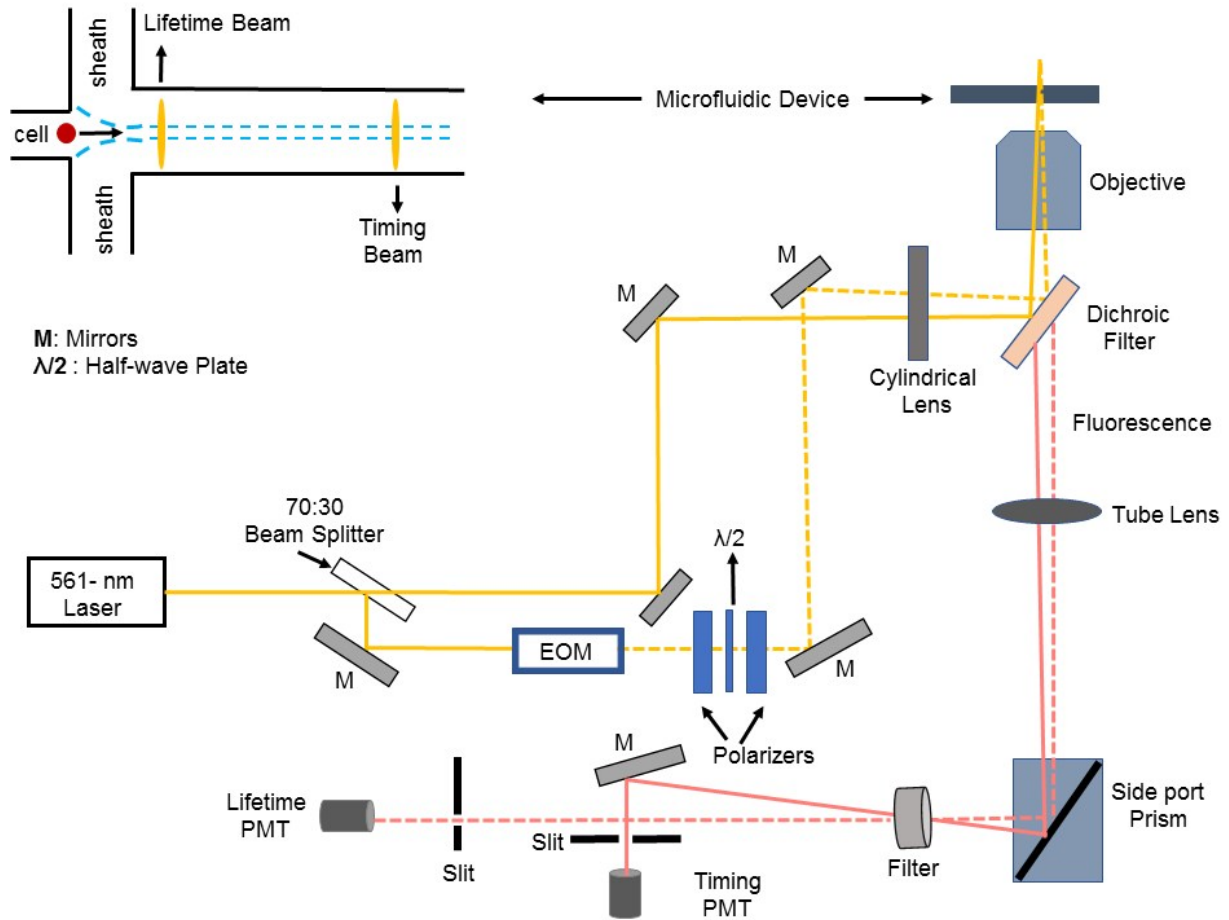


Figure S3: **Schematic of the Optical Layout:** A beam from a 561-nm laser is passed through multiple lenses, mirrors, beam splitters and focused onto the microfluidic chip. The epifluorescence from the RFP-expressing cells upon their passage through the beams are collected using two PMTs. The details can be found in the main text. The trap laser beam is not shown here. Details of the trap laser beam can be found in a previous report by Davis et al.<sup>2</sup>

## Sec. 4. Schematic of the Electronics and Signal Processing

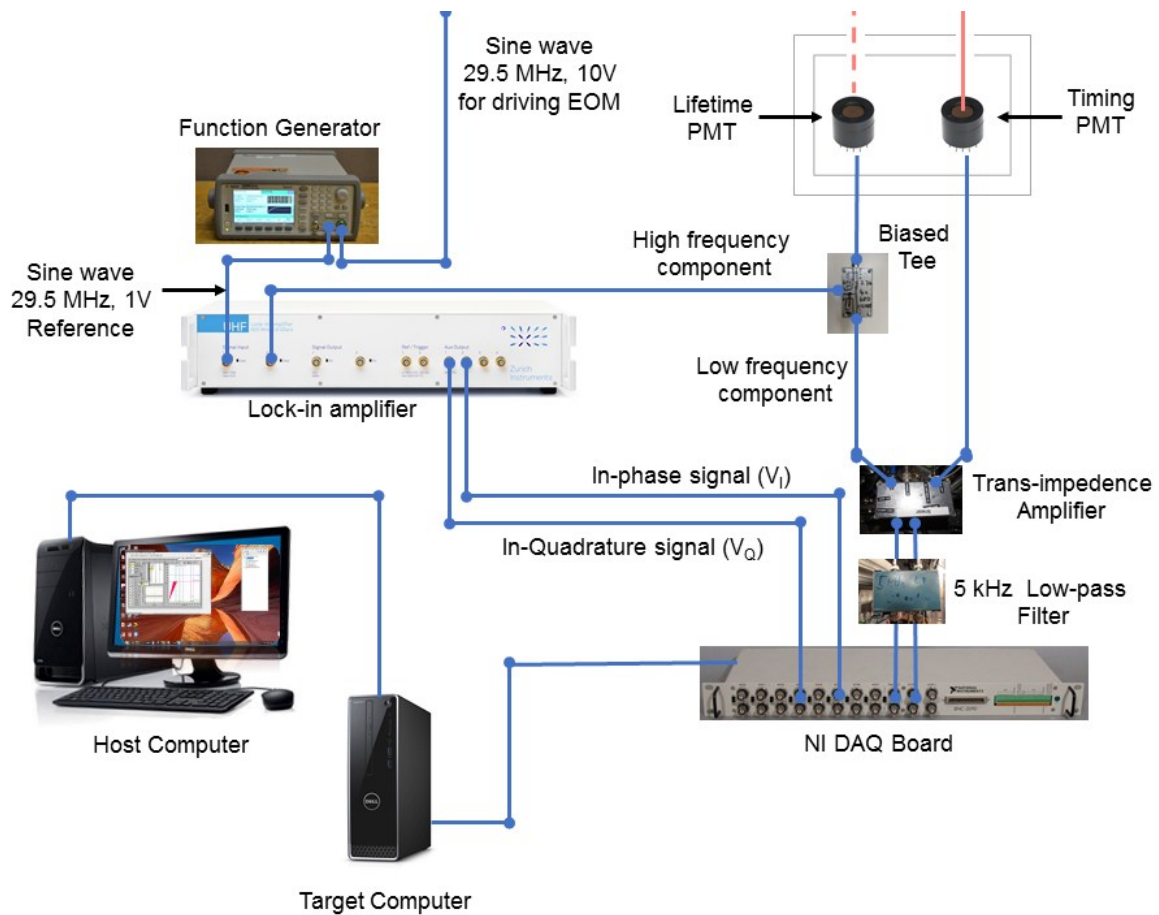


Figure S4: **Schematic of the Electronics and Signal Processing:** Following the collections of red fluorescence from lifetime and timing beams by two red-sensitive PMTs (Hamamatsu R9880U-20), further processing of the signals is conducted by multiple electronics components as described in the main text.

## Sec. 5. Comparative Screening Results Using Linear and Logarithmic Amplifier for Signal Amplification

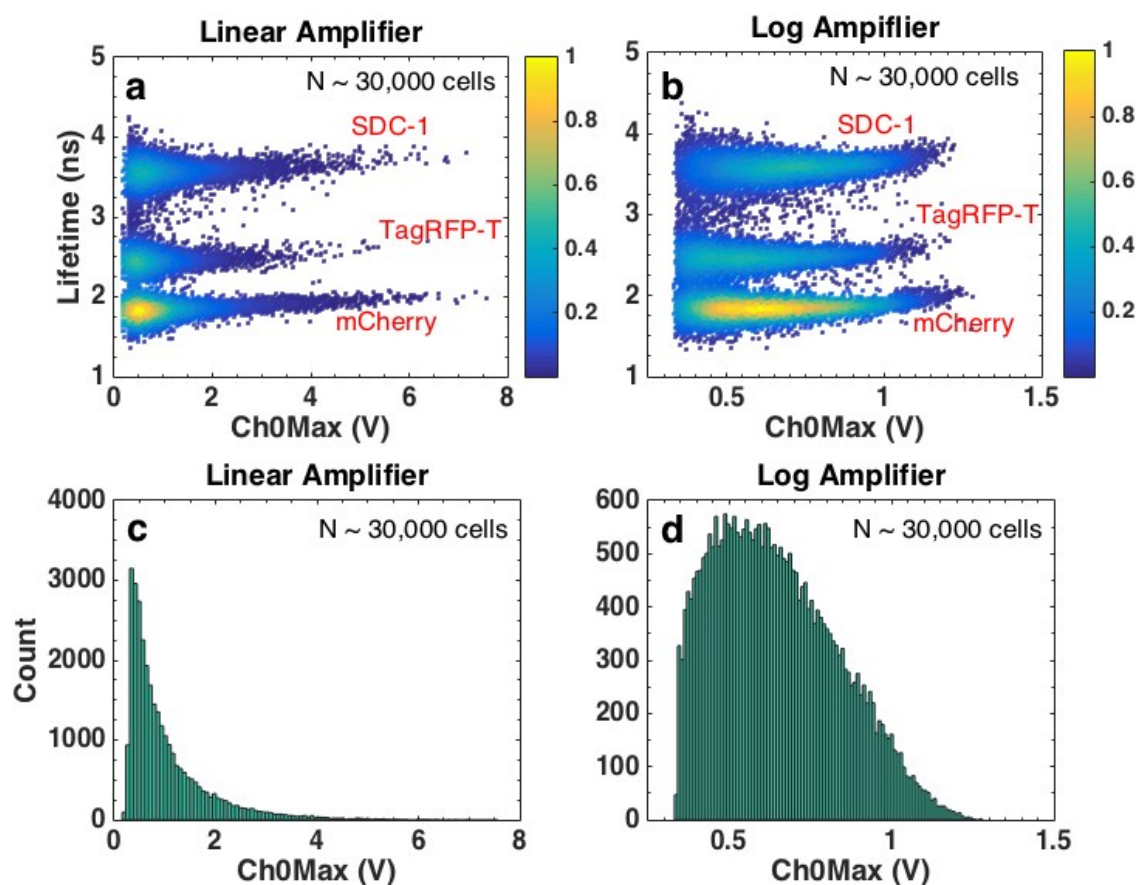


Figure S5: **Microfluidic Screening with Linear and Logarithmic Amplifier:** (a) Microfluidic screening displaying the profile of fluorescence intensity (Ch0Max, fluorescence signal from lifetime beam) and the excited state lifetime of a sample containing mCherry, TagRFP-T and SDC-1 (an unpublished mCherry mutant with mutations of W143M, I161V, Q163L, I197R using mCherry sequence numbering<sup>8</sup>). Linear amplifier was used for the amplification of lifetime PMT signal. (b) Screening results of the same sample using logarithmic amplifier. (c & d) Histogram of Ch0Max of the sample containing mCherry, TagRFP-T and SDC-1 using linear and logarithmic amplifier respectively. ~ 30,000 cells were screened for each run. While both linear and logarithmic amplifier performs equally in measuring the lifetime, owing to its higher dynamic range, logarithmic amplifier captures the peak of the fluorescence intensity distribution of sample which is not possible with linear amplifier. (Pseudocolor indicates normalized cell counts at a certain value of brightness and lifetime on the plot - from yellow indicating the highest till indigo indicating lowest).

It should be noted that the lifetime measured from frequency-domain flow cytometry is approximate in nature. The lifetime results are accurate when the fluorescence lifetime decays of the FPs are purely mono-exponential. For the FPs that display multi-exponential fluorescence decay, only the major component is captured by the frequency-domain lifetime measurements. For instance, fluorescence decay of

mCherry (in purified proteins) when measured in a Time Correlated Single Photon Counting (TCSPC) system shows a bi-exponential decay with a major (73%) 1.74 ns component and a minor (27%) 1.05 ns component. However, in the microfluidic screening of mCherry (in yeast) using the frequency-domain technique, it shows a lifetime of 1.87 ns. This value is close to the value of the major component (1.74 ns) as measured by TCSPC. The slight discrepancy of the values may be attributed to the different environments of the mCherry protein in two different measurement systems (mCherry in yeast for microfluidic & mCherry in purified proteins for TCSPC).



## Sec. 6. Theory of Frequency-Domain Lifetime Measurements in Flow Cytometry

The intensity ( $I(x, y)$ ) of a Gaussian laser beam focused to an elliptical spot with  $1/e^2$  intensity radii  $\sigma_x$  and  $\sigma_y$  is given as <sup>4</sup>

$$I = I_0 \exp\left(-\frac{2x^2}{\sigma_x^2} - \frac{2y^2}{\sigma_y^2}\right), \quad (1)$$

where  $I_0$  is the intensity at the center of the Gaussian beam.

In flow-cytometry, the fluorescence signal generated due to the passage of cells through the laser beam which has a Gaussian profile in temporal coordinate. The peak fluorescence intensity ( $F(t)$ ) of a cell with radius  $r$  and velocity  $v_x$  across the laser beam is given by

$$F(t) = F_0 \exp\left(-\frac{t^2}{2\sigma_t^2}\right), \quad (2)$$

where  $\sigma_t = \frac{\sqrt{\sigma_x^2 + r^2}}{2v_x}$  and the flow is along the x-direction. The fluorescence intensity,  $F_0$ , is proportional to the excitation intensity ( $I(x, y)$ ). Using  $\sigma_x$  as 9  $\mu\text{m}$ ,  $r$  as 3  $\mu\text{m}$  and  $v_x$  as 10 mm/s,  $\sigma_t$  is found to be  $\sim 0.5$  ms. In our measurements, the passage time of the cells in each beam is in the range of 200  $\mu\text{s}$  - 1 ms.

For frequency-domain lifetime measurements, the sample is excited with an amplitude modulated sinusoidal excitation with a period typically on the order of its excited state lifetime. The fluorescence signal emitted by the sample has the same frequency but is phase delayed due to a finite excited state lifetime. So, if the excitation has the form of  $A \sin(\omega t)$ , then the corresponding fluorescence signal would be <sup>1</sup>:

$$A m \sin(\omega t - \phi), \quad (3)$$

where  $A$  is the amplitude of the signal,  $m$  is the modulation,  $\phi$  is the phase shift, and  $\omega$  is the angular frequency of the excitation ( $\omega = 2\pi\nu$ ,  $\nu$  is the modulation frequency). It can be shown that  $\phi$  and  $m$  are related to the excited state lifetime ( $\tau$ ) and angular frequency of the system in the following way <sup>1</sup>:

$$\tau = \frac{1}{\omega} \tan(\phi) \quad (4)$$

$$m = \frac{1}{\sqrt{1 + \omega^2 \tau^2}} \quad (5)$$

In frequency-domain flow cytometry, the fluorescence signal is the product of Eqn. 2

and 3, *i.e.*  $F(t) \propto A m \sin(\omega t - \phi) \exp\left(-\frac{t^2}{2\sigma_t^2}\right)$ . The fluorescence signal is further delayed due to the optics and the electronics used to amplify the signal. The detected signal can be represented as:

$$F(t) \propto A m \sin(\omega t - \phi - \delta) \exp\left(-\frac{t^2}{2\sigma_t^2}\right), \quad (6)$$

where  $\delta$  is the phase shift induced by optics and electronics <sup>5</sup>.

Before the fluorescence signal reaches the lock-in amplifier, the low frequency component ( $\exp\left(-\frac{t^2}{2\sigma_t^2}\right)$ , ~ kHz) is separated from the high frequency component ( $\sin(\omega t - \phi - \delta)$ , ~MHz) using a biased-tee. In the lock-in amplifier, the fluorescence signal is demodulated by multiplying with the reference signal,  $\sin(\omega t)$  and  $\cos(\omega t)$ , to give  $V_I$  and  $V_Q$  respectively. The in-phase signal is then given by:

$$V_I \propto \sin(\omega t - \phi - \delta) \sin(\omega t) \quad (7)$$

$$\propto \frac{1}{2} \cos(2\omega t - \phi - \delta) - \frac{1}{2} \cos(\phi + \delta). \quad (8)$$

The first part of the voltage contribution in the above equation with high frequency can be eliminated using a low-pass filter to give,

$$V_I = B \cos(\phi + \delta) + V_{BI}, \quad (9)$$

where  $B$  is a constant and  $V_{BI}$  is the background signal for the detection of  $V_I$ . Similarly, it can be shown that the quadrature-phase signal ( $V_Q$ ) would be:

$$V_Q = B \sin(\phi + \delta) + V_{BQ} \quad (10)$$

Eqn. 9 and 10 can be rearranged to give

$$\phi = \tan^{-1}\left(\frac{V_Q - V_{BQ}}{V_I - V_{BI}}\right) - \delta. \quad (11)$$

Using Eqn. 4 and Eqn. 11, we get

$$\tau = \frac{1}{\omega} \tan^{-1}\left(\tan^{-1}\left(\frac{V_Q - V_{BQ}}{V_I - V_{BI}}\right) - \delta\right). \quad (12)$$

Further simplification of the above equations gives

$$\tau = \frac{1}{2\pi\nu} \frac{V'_Q \cos(\delta) - V'_I \sin(\delta)}{V'_I \cos(\delta) + V'_Q \sin(\delta)}, \quad (13)$$

where  $V'_I$  and  $V'_Q$  are background corrected in-phase and quadrature-phase signal ( $V'_I = V_I - V_{BI}$ ,  $V'_Q = V_Q - V_{BQ}$ ). Eqn 13 is used for the in-flow quantification of the excited state lifetime of the system.  $V'_I$  and  $V'_Q$  are directly obtained from the lock-in amplifier. The modulation frequency,  $\nu$ , is 29.5 MHz. The parameter  $\delta$  is obtained by using a FP with a known fluorescence lifetime. We use mCherry ( $\tau = 1.87$  ns) as a reference for the adjustment of  $\delta$ .

## Sec. 7. Protocol for Random and Site-directed Mutagenesis

**Error-prone Libraries:** GeneMorph II Random Mutagenesis kit (Agilent Cat No. 200550) was used to create the error-prone libraries. The kit protocol was followed with different amounts of template and cycles depending on the error rate. T7 and V5 universal primers (both located on pYesDest52 vector) were used for the amplification. After first round of PCR, the PCR product was gel-extracted. The gel-extracted PCR product was used for a second round of PCR to create enough DNA for homologous recombination. After PCR purification, the library DNA was isopropanol-precipitated and eluted in a few  $\mu$ l of water.

**Site-directed Mutagenesis:** QuikChange site-directed mutagenesis method was used to make point mutations or switch single amino acids using PfuTurboDNA polymerase and a Thermo cycler. PfuTurboDNA polymerase replicates both plasmid strands with high fidelity and without displacing the mutant oligonucleotide primers. The basic procedure utilizes a supercoiled double-stranded DNA (dsDNA) vector with the FP of interest and two synthetic oligonucleotide primers containing the desired mutation. The oligonucleotide primers, each complementary to opposite strands of the vector, are extended during temperature cycling by PfuTurboDNA polymerase. Incorporation of the oligonucleotide primers generates a mutated plasmid containing staggered nicks. Following temperature cycling, the product is treated with DpnI. The DpnI endonuclease digests the parental DNA template and makes it possible to select for mutation-containing synthesized DNA. The nicked vector DNA containing the desired mutations is then transformed into *E.coli* (Top10).

**Electroporation:** Fresh Competent yeast cells (*Saccharomyces cerevisiae* BY4741) were prepared prior to electroporation. Cells, DNA and cut pYestDest52 vector were combined and left on ice for 5 min. Electroporation conditions (Bio-Rad Gene Pulser Xcell): C = 25  $\mu$ F, PC = 200 ohm, V = 1.5 kV (in 0.2 cm cuvettes). Cells were passed twice prior to expression. Interesting mutants were transferred to pBad-His vector for expression/Ni-NTA protein purification.

## Sec. 8. Characterization of the Single Mutants of FR-13

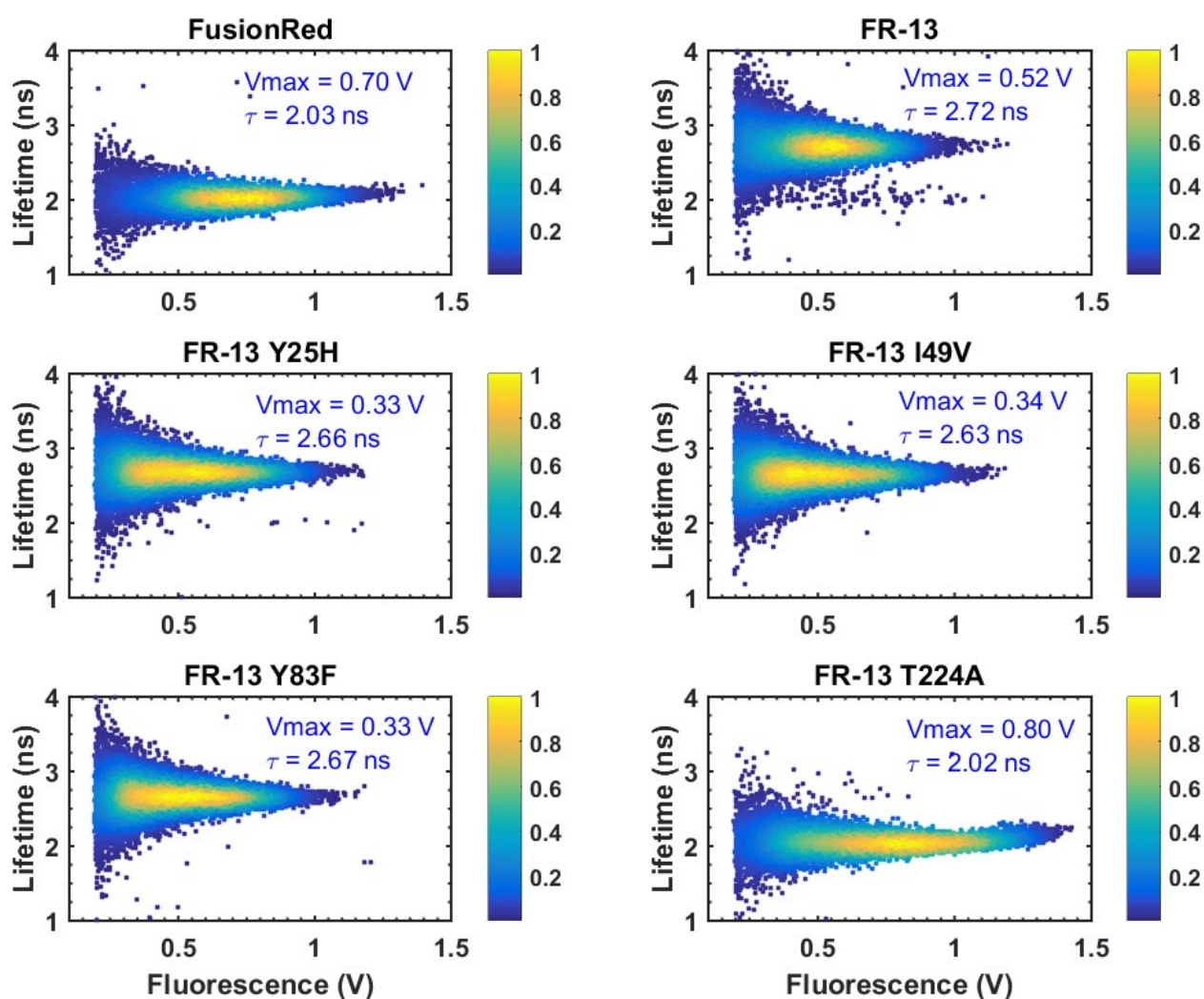


Figure S6: Microfluidic screening results displaying lifetime and brightness (fluorescence signal) of FusionRed, FR-13 and single mutants of FR-13. T224A mutation improved the brightness of FR-13 (fluorescence signal, 0.52 V  $\rightarrow$  0.80 V) while reducing the lifetime (2.72 ns  $\rightarrow$  2.02 ns). This indicates the *in-vivo* brightness of FR-13 and excited state lifetime of FR-13 is controlled by the residue at the position 224. (Pseudocolor indicates normalized cell counts at a certain value of brightness and lifetime on the plot - from yellow indicating the highest till indigo indicating lowest).



## Sec. 9. Evolution of FR-13 Mutant

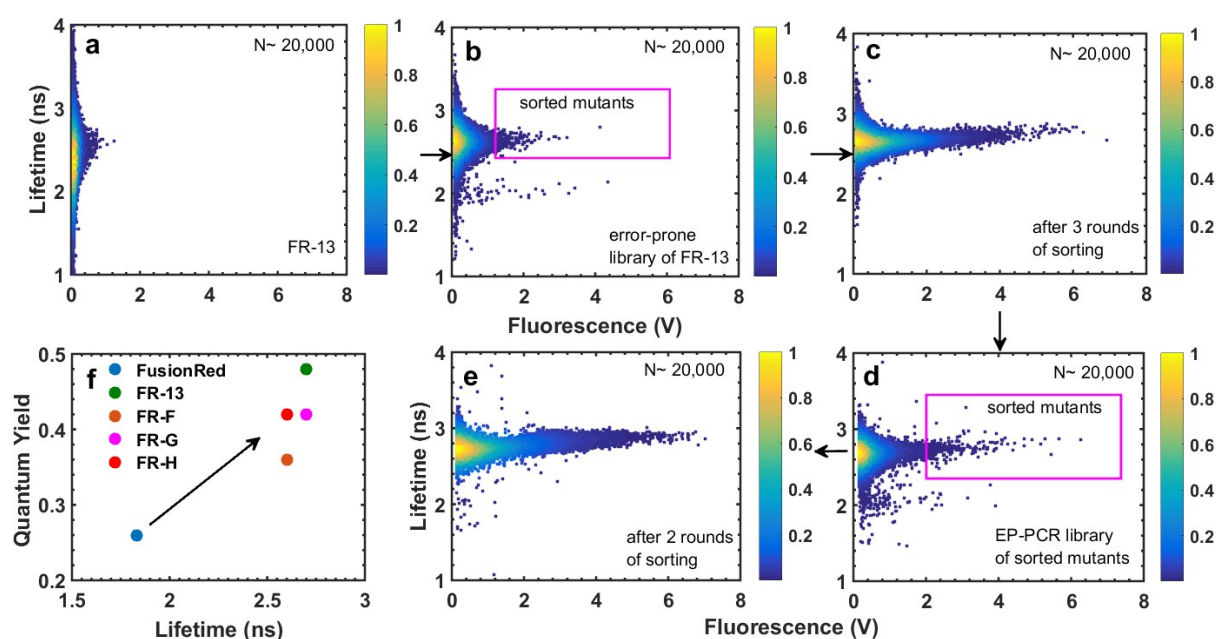


Figure S7: (a-e) Lifetime and brightness (fluorescence signal in volts) profiles of FP libraries displaying the directed evolution of FR-13. To improve the *in vivo* brightness of FR-13, (a) first, it was subjected to a random mutagenesis. Selection of brighter mutants from this error-prone PCR library (b) was carried out with three rounds of microfluidic-based sorting while maintaining the higher lifetime of FR-13. (c) Further random mutagenesis on the sorter-enriched library (d) and subsequent microfluidic enrichment in mutants with higher brightness and longer lifetime (e) were carried out. FR-F, G and H mutants were selected from this sorter-enriched population. (f) Increase in lifetime resulted an enhancement in fluorescence quantum yield for the FusionRed mutants. (Pseudocolor indicates normalized cell counts at a certain value of brightness and lifetime on the plot - from yellow indicating the highest till indigo indicating lowest).

Figure S7 a-e displays the evolution of FR-13 through several random mutagenesis libraries. The first round of EP-PCR mutagenesis and subsequent three rounds of enrichment of brighter mutants through microfluidic sorting generated the FEP library (Figure S7 c). One of the mutants selected from the FEP library, named FEP (FR-13 G160R), showed improved brightness relative to FR-13 and brightness similar to that of FusionRed (Main Text: Figure 3c). Further random mutagenesis on top of the FEP library, followed by two rounds of microfluidic-based enrichment generated multiple mutants brighter than FusionRed wild-type: FR-F, FR-G & FR-H. The *in vitro* photo-physical properties of these mutants are given in Table 1 (main text). The mutants were found to have improved  $\epsilon_{\max}$  and  $\phi$ , resulting in higher *in vitro* brightness. Also, the improved *in vivo* brightness of these mutants suggests that the slow maturation/ lower expression efficiency of FR-13 in yeast is alleviated. Sequencing of these mutants revealed the following mutations relative to FR-13: **FR-F** (V4M, Q115H, L142M); **FR-G** (V4M, G160R, T230S); **FR-H** (V4M, G160R, T230R).

## Sec. 10. Sequence Alignment of the FusionRed Mutants

Residue numbering is based on alignment with avGFP sequence as presented in the literature<sup>6</sup>.

Mutations accumulated in first, second and third round of EP-PCR mutagenesis libraries are highlighted in green, purple and red respectively. Internal residues are highlighted in grey.

	1	4	10	20	25																							
avGFP	M	S	K	G	E	E	L	F	T	G	V	V	P	I	L	V	E	L	D	G	D	V	N	G	H	K	F	S
FusionRed			M	V	S	E	L	I	K	E	N	M	P	M	K	L	Y	M	E	G	T	V	N	N	H	H	F	K
FR-13			M	V	S	E	L	I	K	E	N	M	P	M	K	L	Y	M	E	G	T	V	N	N	Y	H	F	K
FR-F			M	M	S	E	L	I	K	E	N	M	P	M	K	L	Y	M	E	G	T	V	N	N	Y	H	F	K
FR-G			M	M	S	E	L	I	K	E	N	M	P	M	K	L	Y	M	E	G	T	V	N	N	Y	H	F	K
FR-H			M	M	S	E	L	I	K	E	N	M	P	M	K	L	Y	M	E	G	T	V	N	N	Y	H	F	K

*β sheet 1*

	30	40	50																									
avGFP	V	S	G	E	G	E	G	D	A	T	Y	G	K	L	T	L	K	F	I	C	T	T	G	-	K	L	P	V
FusionRed	C	T	S	E	G	E	G	K	P	Y	E	G	T	Q	T	M	R	I	K	V	V	E	G	G	P	L	P	F
FR-13	C	T	S	E	G	E	G	K	P	Y	E	G	T	Q	T	M	R	I	K	V	I	E	G	G	P	L	P	F
FR-F	C	T	S	E	G	E	G	K	P	Y	E	G	T	Q	T	M	R	I	K	V	I	E	G	G	P	L	P	F
FR-G	C	T	S	E	G	E	G	K	P	Y	E	G	T	Q	T	M	R	I	K	V	I	E	G	G	P	L	P	F
FR-H	C	T	S	E	G	E	G	K	P	Y	E	G	T	Q	T	M	R	I	K	V	I	E	G	G	P	L	P	F

*β sheet 2*

*β sheet 3*

	60	70	80																									
avGFP	P	W	P	T	L	V	T	T	F	S	Y	G	V	Q	C	F	S	R	Y	P	D	H	M	K	Q	H	D	F
FusionRed	A	F	D	I	L	A	T	S	F	M	Y	G	S	R	T	F	I	K	H	P	P	G	I	P	-	-	D	F
FR-13	A	F	D	I	L	A	T	S	F	M	Y	G	S	R	T	F	I	K	H	P	P	G	I	P	-	-	D	Y
FR-F	A	F	D	I	L	A	T	S	F	M	Y	G	S	R	T	F	I	K	H	P	P	G	I	P	-	-	D	Y
FR-G	A	F	D	I	L	A	T	S	F	M	Y	G	S	R	T	F	I	K	H	P	P	G	I	P	-	-	D	Y
FR-H	A	F	D	I	L	A	T	S	F	M	Y	G	S	R	T	F	I	K	H	P	P	G	I	P	-	-	D	Y

*α helix 1*

*chromo*

*α helix 2*

	90	100	110																									
avGFP	F	K	S	A	M	P	E	G	Y	V	Q	E	R	T	I	F	F	K	D	D	G	N	Y	K	T	R	A	E
FusionRed	F	K	Q	S	F	P	E	G	F	T	W	E	R	V	T	T	Y	E	D	G	G	V	L	T	A	T	Q	D
FR-13	F	K	Q	S	F	P	E	G	F	T	W	E	R	V	T	T	Y	E	D	G	G	V	L	T	A	T	Q	D
FR-F	F	K	Q	S	F	P	E	G	F	T	W	E	R	V	T	T	Y	E	D	G	G	V	L	T	A	T	Q	D
FR-G	F	K	Q	S	F	P	E	G	F	T	W	E	R	V	T	T	Y	E	D	G	G	V	L	T	A	T	Q	D
FR-H	F	K	Q	S	F	P	E	G	F	T	W	E	R	V	T	T	Y	E	D	G	G	V	L	T	A	T	Q	D

*α helix 3*

*β sheet 4*

*β sheet 5*

	115	120	130																									
avGFP	V	K	F	E	G	D	T	L	V	N	R	I	E	L	K	G	I	D	F	K	E	D	G	N	I	L	G	H
FusionRed	T	S	L	Q	D	G	C	L	I	Y	N	V	K	V	R	G	V	N	F	P	A	N	G	P	V	M	Q	K
FR-13	T	S	L	Q	D	G	C	L	I	Y	N	V	K	V	R	G	V	N	F	P	A	N	G	P	V	M	Q	K
FR-F	T	S	L	H	D	G	C	L	I	Y	N	V	K	V	R	G	V	N	F	P	A	N	G	P	V	M	Q	K
FR-G	T	S	L	Q	D	G	C	L	I	Y	N	V	K	V	R	G	V	N	F	P	A	N	G	P	V	M	Q	K
FR-H	T	S	L	Q	D	G	C	L	I	Y	N	V	K	V	R	G	V	N	F	P	A	N	G	P	V	M	Q	K

*β sheet 6*

*α helix 4*

	140							150							160													
avGFP	K	L	E	Y	N	Y	N	S	H	N	V	Y	I	M	A	D	K	Q	K	N	G	I	K	V	N	F	K	I
FusionRed	K	T	L	-	G	W	E	A	S	T	E	T	M	Y	P	A	-	-	D	G	G	L	E	G	A	C	D	M
FR-13	K	T	L	-	G	W	E	A	S	T	E	T	M	Y	P	A	-	-	D	G	G	L	E	G	A	C	D	M
FR-F	K	T	M	-	G	W	E	A	S	T	E	T	M	Y	P	A	-	-	D	G	G	L	E	G	A	C	D	M
FR-G	K	T	L	-	G	W	E	A	S	T	E	T	M	Y	P	A	-	-	D	G	R	L	E	G	A	C	D	M
FR-H	K	T	L	-	G	W	E	A	S	T	E	T	M	Y	P	A	-	-	D	G	R	L	E	G	A	C	D	M

**$\beta$  sheet 7**  **$\beta$  sheet 8**

	170							180							190													
avGFP	R	H	N	I	E	D	G	S	V	Q	L	A	D	H	Y	Q	Q	N	T	P	I	G	D	-	G	P	V	L
FusionRed	A	L	K	L	V	G	G	G	H	L	I	C	N	L	E	T	T	Y	R	S	K	K	P	A	T	N	L	K
FR-13	A	L	K	L	V	G	G	G	H	L	I	C	N	L	E	T	T	Y	R	S	K	K	P	A	T	N	L	K
FR-F	A	L	K	L	V	G	G	G	H	L	I	C	N	L	E	T	T	Y	R	S	K	K	P	A	T	N	L	K
FR-G	A	L	K	L	V	G	G	G	H	L	I	C	N	L	E	T	T	Y	R	S	K	K	P	A	T	N	L	K
FR-H	A	L	K	L	V	G	G	G	H	L	I	C	N	L	E	T	T	Y	R	S	K	K	P	A	T	N	L	K

**$\beta$  sheet 9**

	200							210							220													
avGFP	L	P	D	N	H	Y	L	S	T	Q	S	A	L	S	K	D	P	N	E	K	R	D	H	M	V	L	L	E
FusionRed	M	P	G	V	Y	N	V	D	H	R	L	E	R	I	K	E	-	A	D	D	E	T	Y	V	E	Q	H	E
FR-13	M	P	G	V	Y	N	V	D	H	R	L	E	R	I	K	E	-	A	D	D	E	T	Y	V	E	Q	H	E
FR-F	M	P	G	V	Y	N	V	D	H	R	L	E	R	I	K	E	-	A	D	D	E	T	Y	V	E	Q	H	E
FR-G	M	P	G	V	Y	N	V	D	H	R	L	E	R	I	K	E	-	A	D	D	E	T	Y	V	E	Q	H	E
FR-H	M	P	G	V	Y	N	V	D	H	R	L	E	R	I	K	E	-	A	D	D	E	T	Y	V	E	Q	H	E

**$\beta$  sheet 10**  **$\beta$  sheet 11**

	224					230										
avGFP	F	V	T	A	A	G	I	T	H	G	M	D	E	L	Y	K
FusionRed	V	A	V	A	R	Y	S	T	G	G	A	G	D	G	G	K
FR-13	V	T	V	A	R	Y	S	T	G	G	A	G	D	G	G	K
FR-F	V	T	V	A	R	Y	S	T	G	G	A	G	D	G	G	K
FR-G	V	T	V	A	R	Y	S	S	G	G	A	G	D	G	G	K
FR-H	V	T	V	A	R	Y	S	R	G	G	A	G	D	G	G	K



## Sec. 11. Photo-physics of the FusionRed Mutants

### Extinction coefficient measurement

The extinction coefficient of FusionRed and FR clones were calculated using the alkali-denaturation method described in the literature<sup>6</sup>. The absorption spectrum of the purified RFP in Tris-HCl buffer (pH=7.4) was measured using Agilent/Varian Cary 500 Spectrophotometer. The same measurement was repeated with same amount of purified RFP in NaOH solution with same volume as previously used Tris-HCl buffer in the same quartz cuvette. The NaOH solution used for FusionRed and its mutants had a pH=14. The denatured FPs exhibit two absorption peaks with known extinction coefficients of  $70,000 \text{ M}^{-1}\text{cm}^{-1}$  near 380 nm ( $\epsilon_{380\text{nm}}$ ) and  $44,000 \text{ M}^{-1}\text{cm}^{-1}$  near 450 nm ( $\epsilon_{450\text{nm}}$ ).<sup>6</sup> The extinction coefficient of RFPs can be calculated by

$$\epsilon_{RFP} = \frac{A_{RFP}}{(A_{380\text{nm}}/\epsilon_{380\text{nm}}) + (A_{450\text{nm}}/\epsilon_{450\text{nm}})}$$

where  $\epsilon$  is the extinction coefficient and  $A$  is the absorbance.

### Fluorescence quantum yield measurement

The quantum yield was measured by the following protocol:

- A series of samples containing the purified RFP (in Tris-HCl buffer with pH=7.4) is prepared with 4-5 different concentrations. The most concentrated sample should exhibit maximum optical density (OD) about 0.2-0.3 measured in a cuvette of 4 cm path length.
- Tris-HCl buffer (pH=7.4) is used for all the dilutions of RFPs.
- Absorption spectra of the samples are measured in Agilent/Varian Cary 500 Spectrophotometer. Baseline corrections are performed for the spectra.
- The emission spectra of the same samples are measured in a QM-6 steady-state fluorimeter from Photon Technology International (PTI). Baseline corrections are performed for the spectra. The cuvette used for emission spectra has 1 cm path length.
- Integrated fluorescence of the samples is quantified by calculating the area under the emission spectra.
- Integrated fluorescence values of the spectra are plotted against the corresponding OD at the wavelength that the series of samples are excited to obtain the emission spectra. In this work we excited the samples at 520 nm to obtain the emission spectra of the RFPs.
- The integrated fluorescence vs. OD plot can be fitted with a straight line of the form:  $y = \text{slope} \times x$ , where  $y$  is the integrated fluorescence and  $x$  is the OD.
- Fluorescence quantum yield of the sample ( $\phi_{\text{sample}}$ ) is computed as:

$$\phi_{\text{sample}} = \frac{\phi_{\text{ref}} \times \text{slope}_{\text{sample}} \times n_{\text{sample}}^2}{\text{slope}_{\text{ref}} \times n_{\text{ref}}^2},$$

where  $n_{sample}$  and  $n_{ref}$  are the refractive index of the sample and the reference, respectively.

- mCherry ( $\phi=0.22$  in Tris-HCl, pH=7.4)<sup>8</sup> or Cresyl violet ( $\phi=0.54$  in EtOH)<sup>9,10</sup> are used as references.

### Excited state lifetime measurement

Excited state lifetimes were measured with a commercial TCSPC system (Fluro Time 100, PicoQuant) using 560-nm laser excitation with a repetition rate of 5 MHz. Lifetime measurements were performed with purified proteins. The fluorescence transients of the FPs were fitted with iterative reconvolution with a bi-exponential function (solid black line) and using the measured instrument function (IRF) of the system (shown in grey). The values of lifetime were obtained by intensity weighted average of the fitted bi-exponential lifetime constants. The results and fitting curves are shown in Fig. S8.

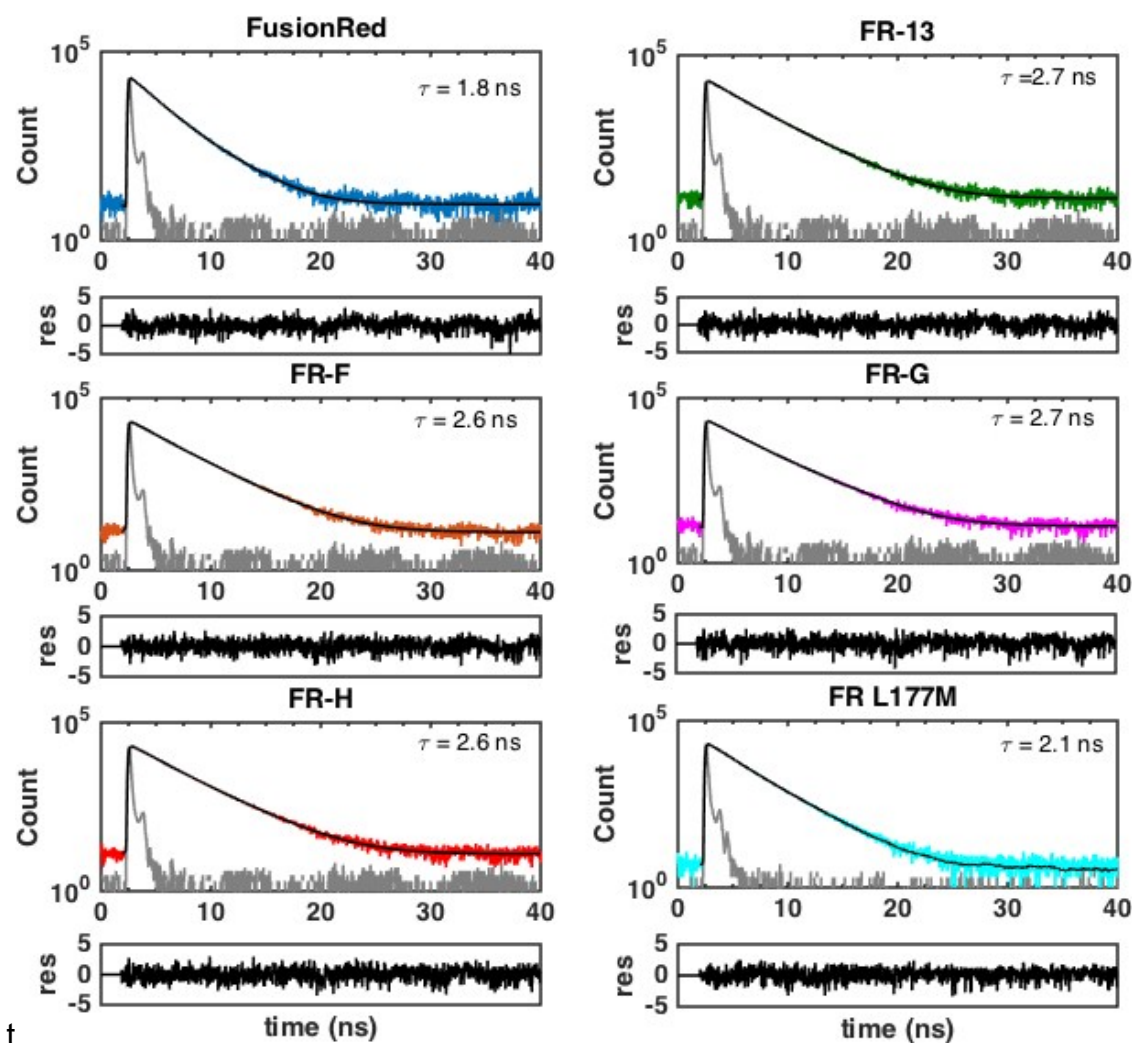


Figure S8: Fluorescence decays of the FusionRed mutants to quantify excited state lifetimes ( $\tau$ ).

## Sec. 12. FACS Screening of Cells Expressing FusionRed Mutants

**Yeast cells** – The FPs were expressed in the cytoplasm of yeast cells (*Saccharomyces Cerevisiae*). After ~18 hours post induction, the cells were suspended in blank media (as described in the main text) and screened for brightness using a commercial FACS setup (BD FACSCelesta). 20,000 yeast cells of each biological triplicate were screened for each run for the quantification of mean brightness ( $\mu$ ). A 561 nm laser was used for excitation and 630/30 nm filter set was used for the detection of red fluorescence. Mean red fluorescence intensities of the mutants from three biological replicates show that FR-F, G and H mutants are brighter than their precursor, FusionRed upon expression in yeast. FR-1 shows a greater improvement in cellular brightness in yeast, hence it was chosen for engineering brighter variants in mammalian cells as an alternate evolution pathway. FR-13 clones underperformed in mammalian cells.

RFP	Mean Brightness - $\mu$ , (Error - $\sigma$ )
FusionRed	100, (21)
FR-13	22, (4)
FR-F	115, (19)
FR-G	131, (8)
FR-H	141, (8)
FR-1	352, (-)
mCherry	190 ,(22)

**Mammalian cells** – The FPs were expressed in the H2B construct of HeLa cells. After ~48 hours post transfection the cells were suspended in blank media and screened for brightness using a commercial FACS setup (BD FACSCelesta). 10,000 HeLa cells for each biological triplicate were screened for each run for the quantification of mean brightness ( $\mu$ ). A 561 nm laser was used for excitation and 630/30 nm filter set was used for the detection of red fluorescence. Mean red fluorescence intensities of FusionRed-M show significant improvement over FusionRed. The L177M mutation inculcates a ~2x brightness in the FusionRed-M mutant in mammalian cells from its precursor FR-1. The FR-13 mutants only exhibit similar brightness as wild-type FusionRed in H2B construct of HeLa cells.

RFP	Mean Brightness - $\mu$ , (Error - $\sigma$ )
FusionRed	100, (54)
FR-1	115, (52)
FusionRed-M	191, (60)
mCherry	180, (45)
FR-F	91, (-)
FR-G	98, (-)
FR-H	138, (-)

## Sec. 13. Maturation Kinetics and Expression level of RFPs

### Measurement of Maturation Kinetics

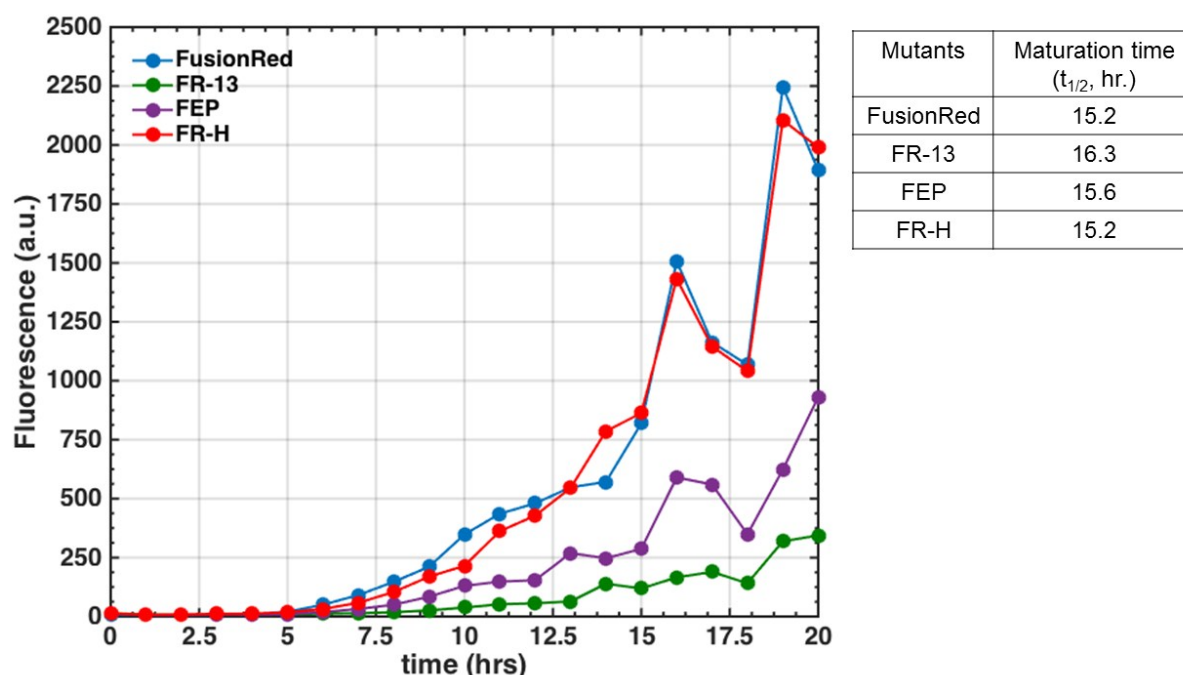


Figure S9: **Maturation kinetics in yeast:** Fluorescence intensities of the FusionRed mutants at different time-points of post-expression. Freshly-grown yeast cultures containing RFP plasmids were induced for expression and incubated at 30°C with continuous shaking at 250 rpm. With 1 hour intervals, 1-2 ml of aliquots were collected from the expression cultures and stored in a -29°C freezer. The cultures continued to express proteins for 20 hrs. and the total volume of the cultures were kept constant by adding an appropriate amount of fresh expression media into the flask containing the cultures. Next, the yeast cultures collected at different time-points were screened in a commercial FACS machine (BD FACSCelesta) with equal number of cell counts (~5000) for quantification of fluorescence. 561 nm excitation and 630/30 nm filter set was used for the screening. Maturation times of the mutants are quantified as the time when the fluorescence intensities are ~50% of the fluorescence recorded after 20 hrs. of post-expression.

### Expression level of RFPs

The cellular brightness measured in FACS screening is a product of molecular brightness and expression level of functional fluorescent protein. The molecular brightness of FusionRed-M exhibited little enhancement comparing to FusionRed as shown in Table 2 in the main text, so we attributed the brightness enhancement of FusionRed-M observed in FACS screening to the improved protein expression level. The cellular brightness will depend on the amount of protein expressed in the cell,

which depends on the efficiency of transcription, stability of mRNA, efficiency of translation, and protein stability, as well as the ability of the protein to fold, mature and produce a function chromophore. We use the cellular brightness measured by FACS as a proxy for protein expression that collectively considers all of these variables. While it is true that individual cells may contain different concentration of the expression plasmid, we examined 10,000 and 20,000 (for HeLa and yeast cells respectively) individual cells and averaged from 3 biological replicates in order to account for this heterogeneity. All FPs were expressed from the same plasmid and transfected in the same way so the heterogeneity due to plasmid concentration would be expected to be similar for the different FPs. The changes in protein expression of FusionRed mutants are estimated as follows. The effective molecular brightness of each FP was calculated by multiplying extinction coefficient at the excitation wavelength (561 nm), quantum yield, and integration of normalized fluorescence spectrum within the emission filter window (630/30 nm, noted as F). The expression level of each FP was obtained by dividing averaged FACS brightness by the effective molecular brightness. The results are normalized with respect to FusionRed and compared with mCherry, the most commonly used RFP, as listed in the table below. The protein expression level was also normalized relative to mCherry shown in red font color.  $\phi$  in the table is the fluorescence quantum yield.  $\epsilon_{561\text{nm}}$  is the extinction coefficient at the excitation wavelength (561 nm) of FACS screening.

	$\epsilon_{561\text{nm}}$ ( $\text{M}^{-1}\text{cm}^{-1}$ )	$\phi$	F	Effective molecular brightness	Mammalian cells			Yeast cells		
					Normalized FACS brightness	Normalized relative expression level	Normalized FACS brightness	Normalized relative expression level	Normalized relative expression level	
mCherry	47,100	0.22	20.63	214,000	180	272	100	190	287	100
FusionRed	71,900	0.26	17.27	323,000	100	100	37	100	100	35
FusionRed-M	63,700	0.34	15.00	325,000	191	190	70	-	-	-
FR-13	10,300	0.48	13.58	673,000	-	-	-	22	11	4

## Sec. 14. OSER Assay

### Cell culture and transfection

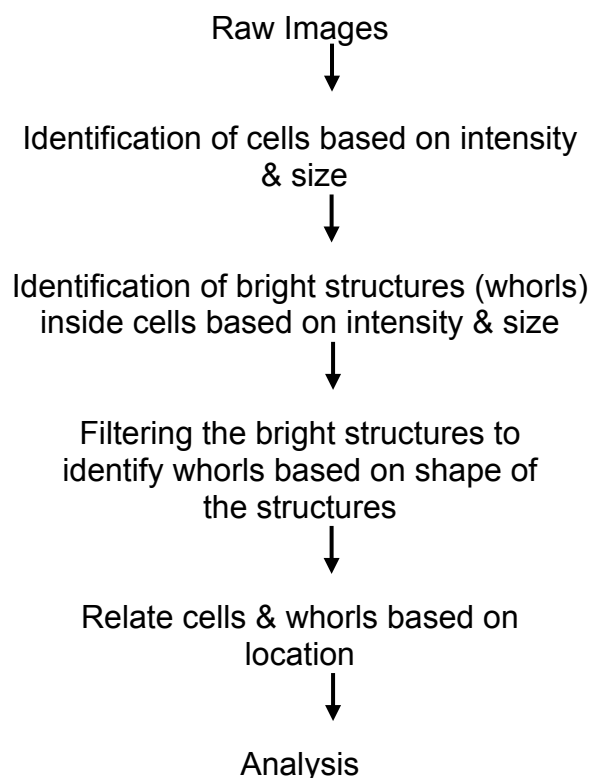
U2OS cells were routinely cultured in RPMI medium (Gibco by Life Technologies), supplemented with penicillin/streptomycin (Gibco by Life Technologies), and 10% heat inactivated fetal bovine serum (Sigma-Aldrich) at 37°C with 5% CO<sub>2</sub> plus humidity. For imaging experiments, cells were grown in 35mm imaging dishes (in-house made using Corning 35x10 mm dishes with VWR 18x18 mm #1.5 cover slips). All CyTERM constructs were transiently transfected for 18-24 hours into cells using Lipofectamine 3000 (Invitrogen) according to the manufacturer's instructions.

### Imaging

Prior to imaging, cells were washed twice with phosphate-free HEPES-buffered Hanks' balanced salt solution (HHBSS) containing 20 mM HEPES (Sigma), pH 7.4. Imaging was conducted in an environmentally controlled chamber (Oko Labs; set to 37°C, 5% CO<sub>2</sub>, 90% humidity) on a spinning disc confocal microscope system (Nikon Ti-E) with a 40x (NA 0.95) air objective. 560 nm laser was used for illumination and 590-650 nm band pass filter (TRITC) was used for the detection of fluorescence with 200 ms exposure time. Several large images ( $\sim 1,680 \times 1,000 \mu m^2$ ) were captured with scanning the z-focus (z-stacks) for optimum focusing of all the cells appeared in the field of view. Typical scanned depth was 5.0 ~ 7.8  $\mu m$  and was evenly separated into 5 ~ 7 layers. Finally, maximum intensity projection of the z-stacks was used for the quantification of OSER score.

## Sec. 15. Program for Analyzing OSER Structures

Here are the details of the analysis program that we have developed for an objective quantification of OSER score (Main Text: Figure 5). The analysis pipeline can be summarized as follows:



For the identification of cells, a binary image was generated by an intensity threshold that discriminates fluorescence from the image background (Figure S10b). In the next step, the cells were identified by:

- using the previously generated binary image as a guide &
- size of the identified objects.

10-50  $\mu\text{m}$  window was used as a size criterion for the cells. Median size of the cells was 20  $\mu\text{m}$ . The program correctly identified cells (green outlines) and rejected the tiny dots (pink outlines) based on size (Figure S10c).

The intensity distribution of the identified cells was measured. Another binary image was generated with using a threshold of:  $\mu_{\text{cell}} + n \cdot \sigma_{\text{cell}}$ , where,  $\mu_{\text{cell}}$  and  $\sigma_{\text{cell}}$  are the mean and standard deviation of the intensity distribution of the cells.  $n$  is an adjustable parameter.  $n=1-2$  works well in our purpose for the identification of bright structures in the cells.  $n=1.5$  was used to generate the binary image 2 (Figure S10d). Bright structures in the cells were identified using the binary image generated in the previous pipeline and based on size criterion. 1-7  $\mu\text{m}$  was used as a size criterion for the OSER structures. The program correctly identifies the bright structures (green outlines) inside the cells (Figure S10e).

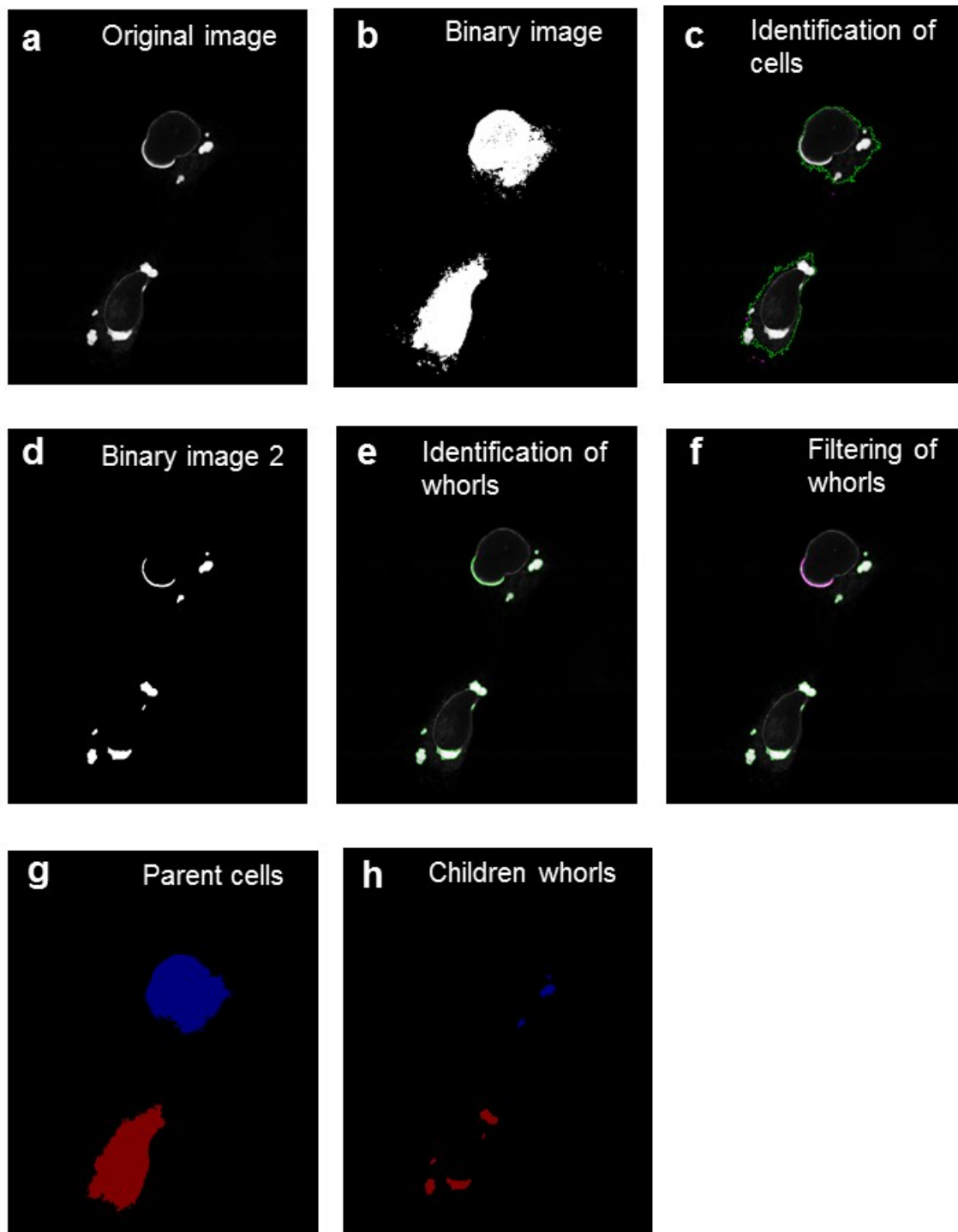


Figure S10: Analysis of the OSER structures. Details of the analysis is given in the text.

In the original OSER article<sup>7</sup>, part of the nucleus having “karmellae” was not considered as whorls. These are nuclear-associated paired membranes produced by over-expression of the enzymes. As “karmellae” s have different shapes than the



whorls, they can be easily filtered out using either eccentricity the form factor (f) of the identified objects. Form factor is defined as follows:

$$f = 4\pi A/p^2$$

where, A and p are the area and perimeter of the structure. A "karmellae" from the cells have been filtered out (shape with pink outline) using a criterion of form factor > 0.25 (Figure S10f).

Structures with roundish shape have been identified as whorls (green outlines). Filtering of whorl based on form factor also eliminates some false positive structures e.g. nice reticular network. Finally, identified whorls & cells are related based on their location. In Figure S10g and S10h, cells were color-labeled with the whorls associated with them.

## REFERENCES:

1. J. R. Lakowicz, *Principles of Fluorescence Spectroscopy*, Springer, **3 rd edn.**, 2006.
2. L. M. Davis, J. L. Lubbeck, K. M. Dean, A. E. Palmer and R. Jimenez, *Lab Chip*, 2013, **13**, 2320-2327.
3. J. L. Lubbeck, K. M. Dean, H. Ma, A. E. Palmer and R. Jimenez, *Anal Chem*, 2012, **84**, 3929-3937.
4. K. M. Dean, L. M. Davis, J. L. Lubbeck, P. Manna, P. Friis, A. E. Palmer and R. Jimenez, *Anal Chem*, 2015, **87**, 5026-5030.
5. M. J. Booth and T. Wilson, *J Microsc-Oxford*, 2004, **214**, 36-42.
6. I. I. Shemiakina, G. V. Ermakova, P. J. Cranfill, M. A. Baird, R. A. Evans, E. A. Souslova, D. B. Staroverov, A. Y. Gorokhovatsky, E. V. Putintseva, T. V. Gorodnicheva, T. V. Chepurnykh, L. Strukova, S. Lukyanov, A. G. Zraisky, M. W. Davidson, D. M. Chudakov and D. Shcherbo, *Nat Commun*, 2012, **3**, 1204(1-7).
7. L. M. Costantini, M. Fossati, M. Francolini and E. L. Snapp, *Traffic*, 2012, **13**, 643-649.
8. N. C. Shaner, R. E. Campbell, P. A. Steinbach, B. N. G. Giepmans, A. E. Palmer and R. Y. Tsien, *Nat Biotechnol*, 2004, **22**, 1567-1572.
9. D. Magde, J. H. Brannon, T. L. Cremers and J. Olmsted III, *J Phys Chem*, 1979, **83**, 696-699.
10. S. J. Isak and E. M. Eyring, *J Phys Chem*, 1992, **96**, 1738-1742.